

Application of extremely compact capillary discharge soft x-ray lasers to dense plasma diagnostics^{a)}

J. J. Rocca,^{b)} E. C. Hammarsten, E. Jankowska,^{c)} J. Filevich, and M. C. Marconi^{d)}
*Department of Electrical and Computer Engineering, Colorado State University, Fort Collins,
Colorado 80523*

S. Moon
Lawrence Livermore National Laboratory, Livermore, California 94550

V. N. Shlyaptsev
Department of Applied Science, University of California Berkeley–Livermore, Livermore, California 94551

(Received 13 November 2002; accepted 7 January 2003)

Table-top capillary discharge soft x-ray lasers combine the advantages of a small size and a high repetition rate with an extremely high brightness similar to that of their laboratory-size predecessors. When utilized to probe high density plasmas their short wavelength results in a higher critical density, reduced refraction, decreased free-electron absorption, and higher resolution as compared to optical probes. These characteristics allow the design of experiments capable of measuring the evolution of plasmas with density–scale length products that are outside the reach of optical lasers. This paper reviews the use of a 46.9 nm wavelength Ne-like Ar capillary discharge table-top laser in dense plasma diagnostics, and reports soft x-ray laser interferometry results of spot-focus Nd:YAG laser plasmas created at moderate irradiation intensity ($\sim 7 \times 10^{12} \text{ W cm}^{-2}$) with ~ 13 ns pulse width duration laser pulses. The measurements produced electron density maps with densities up to $0.9 \times 10^{21} \text{ cm}^{-3}$ that show the development of a concave electron density profile that differ significantly from those of a classical expansion. This two-dimensional behavior, that was recently also observed in line-focus plasmas, is analyzed here for the case of spot-focus plasmas with the assistance of hydrodynamic model simulations. The results demonstrate the use of a table-top soft x-ray laser interferometer as a new high resolution tool for the study of high density plasma phenomena and the validation of hydrodynamic codes. © 2003 American Institute of Physics.
[DOI: 10.1063/1.1557056]

I. DENSE PLASMA DIAGNOSTICS WITH TABLE-TOP SOFT X-RAY LASERS

Optical lasers have been used for decades to diagnose dense plasmas utilizing techniques that include interferometry, deflectometry, shadowgraphy and scattering.¹ However, the maximum plasma density and size that can be studied are limited by plasma refraction of the probe beam, by free–free absorption, and in the case of interferometry by the maximum number of fringe shifts that can be detected experimentally.² Nevertheless, since all these limitations decrease as a function of the frequency of the probe beam, the use of shorter wavelength laser probes can significantly extend the plasma parameter space that can be probed. The short wavelength and high peak spectral brightness of soft x-ray lasers make them ideal sources for probing high density plasmas. Their shorter wavelength amounts to a higher critical plasma density for the probe beam that results in reduced refraction. The shorter wavelength also results in

smaller diffraction and allows for higher resolution. Moreover, their high monochromaticity allows for the use of multilayer-coated optics as filters to discriminate the probe beam from the strong self-emission of the hot dense plasmas.

The first soft x-ray laser plasma diagnostics experiments were conducted at Lawrence Livermore National Laboratory using a laboratory-size 15.5 nm Ne-like Y laser pumped by the Nova laser. These experiments included shadowgraphy and radiography,³ Moire deflectometry,⁴ and interferometry^{2,5} of dense large-scale plasmas. The studies provided insight into dense plasma phenomena unavailable through other techniques in spite of the low repetition rate (limited to several shots per day) and the high complexity of the laboratory x-ray laser probe. Table-top soft x-ray lasers⁶ combine the advantages of a much higher repetition rate and a small compact size with an extremely high brightness that in some cases is similar to or higher than that of their laboratory-size predecessors. These characteristics allow the design of plasma diagnostic experiments that can systematically measure the evolution of high-density plasmas, providing data for the validation of hydrodynamic codes. The capillary discharge pumped soft x-ray lasers described in Sec. II offer the opportunity to develop portable soft x-ray tools for the diagnostics of a large variety of dense plasmas. Some of us have utilized a 46.9 nm capillary discharge Ne-like Ar

^{a)}Paper GI2.5, Bull. Am. Phys. Soc. **47**, 138 (2002).

^{b)}Invited speaker.

^{c)}Permanent address: Department of Physics, Wrocław University of Technology, Poland.

^{d)}Also with the Department of Physics, University of Buenos Aires, Argentina.

laser to realize the first demonstrations of plasma shadowgraphy⁷ and interferometry with a table-top soft x-ray laser source.^{8–12} More recently, a compact laser-pumped transient collisional x-ray laser operating at 14.7 nm was used to obtain interferograms of a laser-created plasma with picosecond resolution.¹³ In Sec. III we discuss the experimental techniques developed to conduct soft x-ray laser interferometry of dense plasmas and presents results of the study of two-dimensional effects in laser-created plasmas.

II. COMPACT CAPILLARY DISCHARGE COLLISIONAL SOFT X-RAY LASERS

There are strong motivations for the development of compact soft x-ray lasers for dense plasma diagnostics and other applications. Collisionally excited table-top lasers based on fast discharge excitation^{14,15} and short pulse laser excitation^{16,17} have both reached gain saturation. Lasing by collisional recombination in transitions to the ground state has also been demonstrated in a table-top setup.¹⁸ Capillary discharge excitation of elongated Ne-like Ar plasma columns has produced laser pulses with energies approaching one mJ and mW average powers of coherent radiation at 46.9 nm in a table-top setup. Large amplification with this excitation technique has also been demonstrated at 52.8 nm in Ne-like Cl¹⁹ and at 60.2 nm in Ne-like S.²⁰

In the 46.9 nm Ne-like Ar discharge-pumped laser the amplification is generated by excitation of an Ar-filled capillary channel with a fast discharge current pulse. Prior to the arrival of the fast current pulse, the gas in the capillary channel is seeded with a significant density of free electrons and ions created by a pre-ionizing current pulse of $\sim 1 \mu\text{s}$ duration that reaches ~ 80 A amplitude. In this excitation scheme the magnetic force of the fast current pulse rapidly compresses the plasma to form a dense and hot column with a large density of Ne-like ions, a very high axial uniformity, and length to diameter ratio exceeding 1000:1. Collisional electron impact excitation of the ground state Ne-like ions produces a population inversion between the $3p$ (1S_0) and $3s$ ($^1P_1^0$) levels, resulting in the amplification at 46.9 nm.²¹ Figure 1 illustrates the simulated dynamics of an Ar plasma column created in a 3.2 mm diameter capillary filled with 460 mTorr of Ar and excited by a fast current pulse of 25 kA peak amplitude and 25 ns risetime. The spatio-temporal evolution of the electron temperature and plasma density computed with the code RADEX²² is shown. A shock wave originates in the vicinity of the capillary wall and is accelerated towards the center by the Lorentz force and large thermal pressure gradients near the wall. A heat wave moves ahead of the mass. When the heat wave arrives at the axis, the maximum current density and Joule dissipation switches to the center of the discharge. A plasma column 200–300 μm in diameter with peak electron temperature of about 100 eV is formed. Lasing occurs at a time when the electron temperature is 60–80 eV.²³ The electron density peaks a few ns later, exceeding $1 \times 10^{19} \text{ cm}^{-3}$. The total current flowing inside the compressed plasma column is only 15–20% of the total current. This situation probably helps to suppress current instabilities.²⁴ Thus, the very good initial plasma symmetry

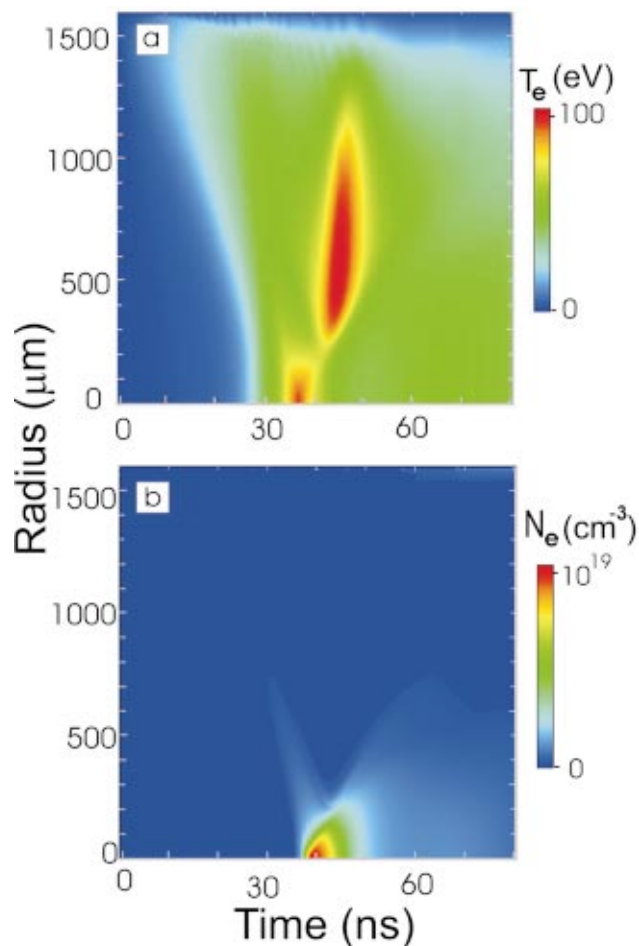


FIG. 1. (Color) Simulated spatio-temporal distribution of the (a) electron temperature and (b) electron density in a capillary discharge argon plasma column. The calculation is for an alumina capillary 3.2 mm diameter filled with 460 mTorr of Ar excited by a current pulse with a peak amplitude of 25 kA and 30 ns rise time.

of the pre-ionized plasma column, and the relatively short time duration of the compression process are all likely to contribute to the suppression of the instabilities that commonly deteriorate the symmetry of many high current discharges. The very good axial uniformity of these plasma columns is evidenced by the excellent measured spatial coherence of the amplified beam.²⁵

In the capillary laser devices that have produced the highest output pulse energies and average powers the discharge takes place in aluminum oxide capillary channels 3.2 mm in diameter and up to 36 cm in length, filled with pre-ionized Ar gas at a pressure of 490 mTorr. The plasma columns are excited by current pulses of ~ 26 kA peak amplitude, with a 10% to 90% rise time of approximately 40 ns. The excitation current pulse is produced by discharging a water capacitor through a spark gap switch connected in series with the capillary load. The water serves as a liquid dielectric for the capacitor and also is circulated to cool the capillary for repetitive operation. The capacitor is pulse-charged by a compact four-stage Marx generator. The compact typical size of such a capillary discharge Ne-like Ar laser is illustrated at the right of Fig. 2, as part of the setup



FIG. 2. Setup for soft x-ray laser plasma interferometry experiments. The capillary discharge soft x-ray laser observed on the right of the photograph generates a 46.9 nm wavelength beam that propagates into the amplitude division soft x-ray interferometer seen at the left. A commercial 1 J Nd:YAG laser used to generate the laser-created plasmas studied is seen in the lower part of the figure.

used to conduct soft x-ray interferometry in laser-created plasmas. A commercial 0.8 J Nd:YAG laser used to create the plasmas that are the subject of the plasma characterization experiments described in Sec. III can be seen on the lower part of the figure. The capillary discharge soft x-ray laser has a size comparable to the Nd:YAG laser and occupies a table space of approximately $0.4 \text{ m} \times 1 \text{ m}$.

Efficient energy extraction is obtained by operating the laser in a highly saturated regime. The laser pulse intensity increases nearly exponentially as a function of plasma column length, until it reaches the gain saturation intensity of $56\text{--}78 \text{ MW cm}^{-2}$ at a plasma column length of about 14 cm. As the laser pulse propagates beyond this point in the plasma columns, its intensity reaches the linear amplification regime that characterizes a saturated amplifier. Laser output pulses for the longest capillaries used (36 cm) exceed the saturation intensity by more than an order of magnitude, approaching 1 GW cm^{-2} . Correspondingly, the laser pulse energy was measured to increase linearly with length from 0.075 mJ for a plasma column 16 cm in length, to 0.88 mJ ($>2 \times 10^{14}$ photons/pulse) for a plasma column length of 34.5 cm. Average laser powers of 3.5 mW and a peak power of 0.6 MW were obtained operating the laser at a repetition rate of 4 Hz. More than 5000 laser shots were generated using a single capillary. The full width at a half maximum laser pulse width measured for the longest capillaries is $1.5 \pm 0.05 \text{ ns}$.¹⁴ This laser pulse width is longer than the 1.2 ns that was measured for an 18.2 cm long amplifier.¹⁵

Recent measurements demonstrated that full spatial coherence is approached with the longest capillaries and that the peak spectral brightness is about 2×10^{25} photons/(s mm² mrad² 0.01 % bandwidth).²⁵ This value makes this table-top laser one of the brightest soft x-ray sources available. A series of Young's interference experiments measured a rapid increase of the spatial coherence as a function of capillary length. This coherence buildup is the result of strong refractive anti-guiding and gain guiding taking place in the capil-

lary plasma column. At the discharge conditions mentioned above the plasma column acquires an electron density profile that presents a maximum density on axis at the time of maximum amplification. The associated variation of the refractive index refracts the amplified beam, causing a ring shaped intensity distribution in the far field with a peak to peak divergence of about 4.6 mrad. With the presence of significant refraction only radiation that propagates near the axis experiences substantial gain and contributes to the output of the laser. Therefore, at the expense of the effective gain, refraction provides a mode selection mechanism that significantly improves the spatial coherence of the soft x-ray laser for long plasma columns. This intrinsic mode selection mechanism makes it possible to achieve a coherence radius comparable to the beam size. Such a high spatial coherence allows us to obtain high contrast interferograms for dense plasma diagnostics.

III. SOFT X-RAY LASER INTERFEROMETRY OF DENSE PLASMAS

The power of interferometry as a plasma diagnostic technique resides in its ability to generate detailed maps of the electron density without having to rely as heavily on modeling as other techniques. Da Silva *et al.* conducted soft x-ray laser interferometry experiments using a laboratory-size 15.5 nm Ne-like Y laser in conjunction with a Mach-Zehnder interferometer based on thin-film beam splitters.²⁶ To realize demonstrations of soft x-ray interferometry of dense plasmas with a table-top laser, we used the 46.9 nm capillary discharge laser in combination with either a wavefront-division interferometer based on Lloyd's mirror,^{8,9} or an amplitude division interferometer in which diffraction gratings were used as beam splitters.^{10,11} Other soft x-ray laser interferometers based on a Fresnel bimirror²⁷ and a Michelson interferometer that makes use of a thin film beam splitter²⁸ have been demonstrated or are under development by other groups.

The Lloyd's mirror is the simplest possible reflection interferometer, and because it is based on a grazing incidence reflection it is particularly well suited for soft x-ray interferometry. In a previous publication we have discussed a proof of principle interferometry experiment in which a Lloyd's mirror and a 46.9 nm capillary discharge laser were used to measure the electron density distribution in the cathode region of a pinch plasma.^{8,9} While simplicity is an advantage of the Lloyd's mirror interferometer, the diffraction grating interferometer (DGI) described below has the advantage of producing interferograms of significantly higher quality, which display a high fringe visibility (~ 0.5) over the entire field of view.

A. High throughput amplitude division soft x-ray laser interferometer based on diffraction gratings

The DGI (illustrated in Fig. 3) is a high throughput amplitude division interferometer design that can be adapted for operation with any of the presently available saturated soft x-ray lasers. It consists of a Mach-Zehnder configuration of rhomboidal shape in which the beam splitters are gold coated diffraction gratings.¹⁰ The zero and first diffracted orders

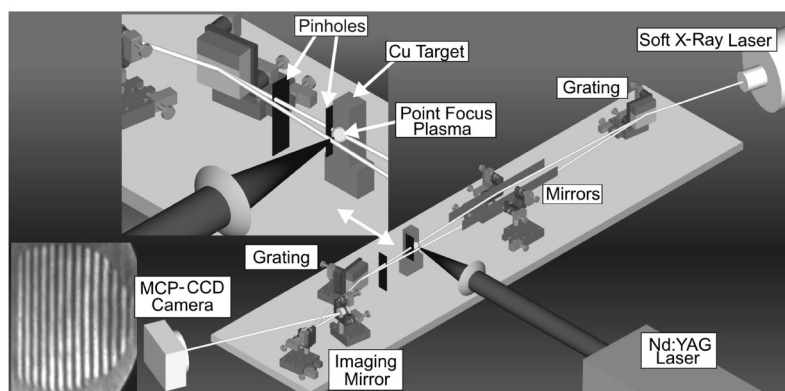


FIG. 3. A schematic representation of the amplitude division soft x-ray laser interferometer based on diffraction gratings. The interferometer was positioned ~ 2 m from the exit of the soft x-ray laser. The detector was placed ~ 7 m from the interferometer. An interferogram obtained with no plasma present is shown.

from the first grating are used to form the two arms of the interferometer. For operation at 46.9 nm diffraction gratings with a line density of 300 lines per mm and an angle of incidence of 79 degrees were selected. The blaze angle of the gratings is chosen to split the laser beam into two beams of nearly equal intensity. Two elongated gold coated mirrors placed at a grazing incidence angle of 88.2 degrees redirect the beam towards the second grating where they are recombined and the interference pattern is generated. By changing the angle and inclination of the mirrors and the second grating the fringe spacing and orientation can be modified according to the requirements of each particular experiment. The plasma to be studied is introduced in the path of the zeroth order beam between the grazing incidence mirror and the second grating. Advantages of the DGI scheme over other amplitude-division soft x-ray interferometers based on thin film beam splitters^{2,28} include a higher throughput ($\sim 6\%$ percent per arm) and a significantly increased resistance of the beam splitters to plasma debris. Moreover, as mentioned above the DGI can also be designed to operate at different soft x-ray wavelengths by choosing gratings with the proper ruling and blaze angle. In contrast, the operation of interferometers based on thin film beam splitters is limited to wavelengths where material absorption is low, which, for example, excludes their use with the 46.9 nm Ne-like Ar laser. Recently a version of this DGI designed to operate at a wavelength of 14.7 nm was combined with a Ni-like Pd transient soft x-ray laser to successfully demonstrate picosecond-resolution soft x-ray interferometry of dense laser-created plasmas.¹³

While all key movements of the interferometer are motorized to allow for optimization of the alignment under vacuum, the initial alignment is performed at atmospheric pressure using an 824 nm wavelength diode laser having the coherence length similar to that of the Ne-like Ar soft x-ray laser ($\sim 200 \mu\text{m}$). The gratings were ruled with two vertically displaced sets of lines to make possible the alignment of the interferometer with the 824 nm semiconductor laser. Line densities of 300 lines/mm for the soft x-ray laser beam and 17.06 lines/mm for the infrared laser beam were ruled.²⁹ In the experiments discussed below a flat relay mirror and a spherical imaging mirror, both coated with Si/Sc multilayers with reflectivity of $\sim 40\%$ at 46.9 nm,³⁰ were used to image the plasma onto a gated two-dimensional detector setup with

a magnification of either 25 or $51\times$. The detector was constructed combining an MCP, a phosphorous screen, and a one inch x one inch, 1024×1024 pixel CCD. To improve the fringe contrast in the presence of the plasma self-emission we exploited the high degree of collimation of the soft x-ray laser beam by utilizing a set of pinholes ~ 1 mm in diameter (see Fig. 3). This allowed us to significantly reduce the amount of plasma radiation collected by the detector. The amount of plasma radiation collected by the imaging system was further reduced by gating the MCP for 4–5 ns using a fast high voltage pulse.

B. Study of two-dimensional effects in a spot-focus laser-created plasma

Measurements of the electron density distribution in laser-plasmas created by irradiating solid targets at moderate intensities ($< 10^{13}$ W/cm²) normally show plasma profiles that are well described by one-dimensional (1-D) hydrodynamic models that adjust the angle of expansion, often described as $1\frac{1}{2}$ -D models. At higher irradiation intensities ($> 10^{14}$ W/cm²) the radiation pressure can be sufficiently large with respect to the plasma pressure to significantly alter the electron density profile by excluding the plasma from regions of otherwise high density.^{31–33} In recent soft x-ray laser interferometry studies of seemingly typical laser-plasmas, where the ponderomotive force and other effects associated with high irradiation intensities are negligible, we observed¹¹ plasma density distributions that differ significantly from the expected classical conical expansion. That investigation was conducted using the DGI soft x-ray laser setup described above to map the dynamics of a line-focus plasma created by irradiation of a polished Cu slab target with $\lambda = 1.06 \mu\text{m}$ Nd:YAG laser pulses of ~ 13 ns FWHM duration. The line-focus, which was created using the combination of a cylindrical and a spherical lens, was measured to be $\sim 30 \mu\text{m}$ in width and 1.8 mm in length by imaging the target surface onto a CCD camera. The irradiation intensity was $\sim 1 \times 10^{11}$ W/cm². Interferograms corresponding to early times during the laser pulse show a convex electron density profile. However, starting at about 6 ns after the initiation of the laser pulse the interferograms revealed the formation of a concave electron density distribution with pronounced plasma sidelobes and a local minimum on the

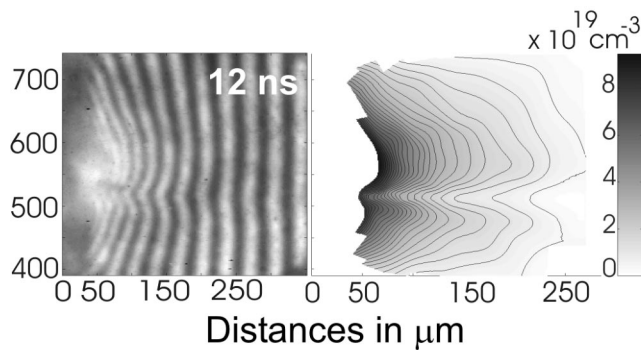


FIG. 4. An on-axis interferogram of line-focus plasma generated by irradiation of a copper target with an intensity of $\sim 1 \times 10^{11} \text{ W cm}^{-2}$ (left), and corresponding electron density profile (right). The width of the line focus was $30 \mu\text{m}$.

irradiation axis that cannot be modeled using 1-D simulations (Fig. 4). Hydrodynamic simulations showed that the observed two-dimensional profiles are caused by the generation of cold plasma sidelobes outside the laser-irradiated target area and by the subsequent establishment of pressure balance that results in the observed axial density minima.¹¹ The sidelobes result from the build-up of cold material generated by an increased ablated area caused mainly by XUV plasma radiation. The simulations indicated that this is essentially a universal effect that should be observed over a relatively wide range of plasma parameters. A review of the literature shows that a similar behavior can be inferred from plasma created at different excitation conditions than those discussed herein.^{34,35} However, this phenomenon was not previously studied in detail nor was it completely understood. The low refraction of the soft x-ray laser probe allowed us to measure line-focus plasma where the two-dimensional effects can be clearly observed and analyzed without having to resort to an Abel inversion of the data. It should be noticed that probing of such dense elongated plasma is outside the plasma parameter range that can be probed with optical lasers. This is illustrated in Figs. 5(a) and 5(b), where the computed ray trajectories corresponding to a 355 nm optical laser probe (third harmonic of Nd:YAG) are compared with those of a 46.9 nm capillary discharge laser beam. Refraction is observed to strongly deflect and intermix the rays of the optical probe beam, while it only has a small effect on the trajectory of the soft x-ray laser probe.

In the present paper we extend the study of the two-dimensional dynamics of laser-created plasmas generated at moderate irradiation intensities into the case of spot focus plasmas. The plasmas were created by focusing 0.62 J pulses from a Nd:YAG laser ($\lambda = 1.06 \mu\text{m}$, 13 ns FWHM duration) with an $f = 15 \text{ cm}$ aspheric lens into a $\sim 30 \mu\text{m}$ diameter spot to generate laser intensities of $\sim 7 \times 10^{12} \text{ W cm}^{-2}$. The target consisted of a 99.99% pure copper disk that could be rotated around its axis using a motorized stage, allowing access to approximately 200 target locations without having to break vacuum. Detailed series of soft x-ray interferograms were obtained by irradiating either a new target area or a previously irradiated area. Interferograms of plasmas created by firing a first, second or fifth laser shot in the same target

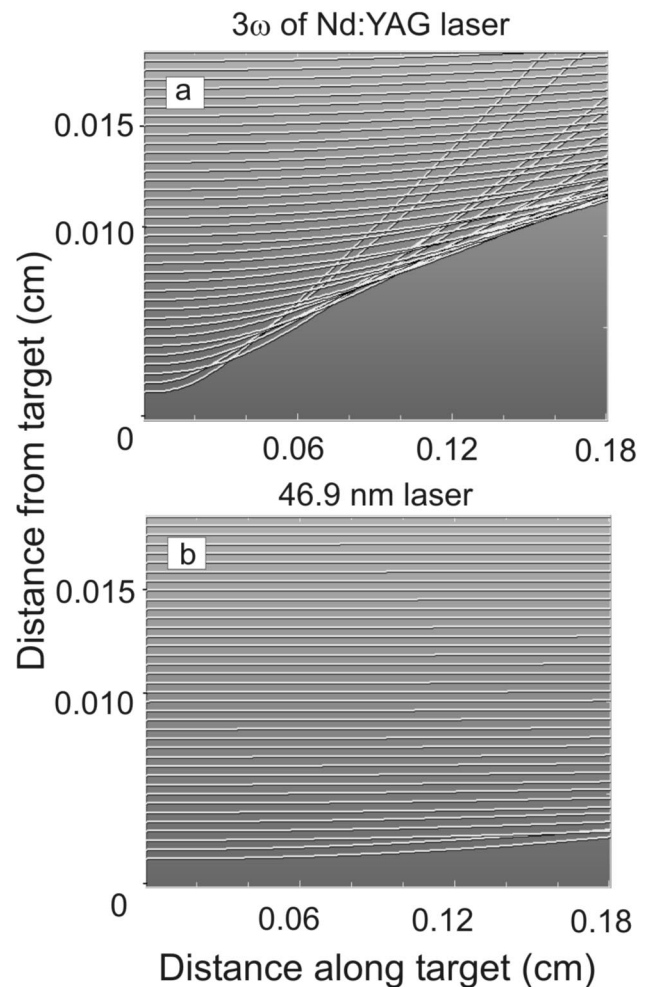


FIG. 5. Computed ray trajectories of a probe beam propagating along the axis of a line-focus plasma corresponding to the interferogram of Fig. 4 for (a) third harmonic of Nd:YAG laser, (b) 46.9 nm soft x-ray laser.

location were obtained using $51\times$ magnification. The interferograms corresponding to a first shot show the high density plasma region extends only a few tens of microns away from the target. In contrast, the plasmas produced firing multiple laser shots in the same target location are observed to cover a significantly larger volume, with large electron densities at distances of more than a hundred micrometers from the target. The larger extent of the plasmas results from the fact that they emanate from the crater created by the previous shots (a single pre-shot on target for the second shot series, or four pre-shots for the fifth shot series). Previous studies of laser-created plasmas have recognized that plasma characteristics can be influenced by the presence of a crater.^{35,36} The crater constrains the lateral expansion and guides the plasma motion into the direction normal to the target. The crater formed on the target after the fifth shot is observed to have relatively vertical walls, a depth of $\sim 300 \mu\text{m}$, and a diameter of $\sim 200 \mu\text{m}$. In these cases the amount of plasma generated is substantially increased by the larger ablation caused by the higher temperature, the increased contact of plasma with the crater's wall and by the increased XUV emission efficiency at higher densities. In all three cases the interferograms

present a flattening or reversal of the curvature of the interference fringes near the irradiation axis. In this axisymmetric geometry such fringe patterns are indicative of a concave electron density profile with a minimum on axis (a probe ray intercepting the axis transverses a maximum length of plasma, undergoing a maximum phase shift unless there is a density depression or cavity). At the time of the maximum laser intensity this central minimum in the density profile is observed to extend through a significant part of the subcritical region of the plasma. It should be noticed that this concave electron density profile was observed in the first shot in spot focus as well as in line focus targets, and is therefore not a result of the crater created by previous shots on target.

Figure 6 shows a sequence of interferograms corresponding to plasmas generated by firing the laser a fifth time on the same target location. The time relative to the initiation of the heating laser pulse is indicated. The fringes closer to the target are observed to develop a concave shape, corresponding to a density depression on axis. This density cavity becomes more pronounced as time progresses towards the maximum of the heating laser pulse. An Abel inversion was performed to deconvolve the radial electron density distribution from these axisymmetric interferograms. The electron density distributions derived from Abel inversion of the interferograms of Fig. 6 are shown in Fig. 7. The formation of a concave electron density profile with a pronounced plasma sidelobe and a density cavity on the irradiation axis is observed. A series of interferograms obtained for plasmas generated by firing a second shot in the same target location shows qualitatively similar density profiles and temporal evolution. In that case the electron density in the sidelobes was observed to increase as a function of time, to reach a maximum density $\sim 9 \times 10^{20} \text{ cm}^{-3}$ (90% of the critical density) at a distance of $27 \mu\text{m}$ from the target surface near the time of maximum laser irradiation intensity.

C. Simulation and discussion

The hydrodynamic code LASNEX³⁷ was used to simulate the plasmas studied by soft x-ray laser interferometry. Figure 8 shows the computed evolution of the electron density and temperature profiles for the spot-focus plasma of Fig. 6. The simulations were performed for a 0.65 J and 13 ns FWHM 1ω Gaussian light pulse, with a spot size of $30 \mu\text{m}$ diameter focused at the origin ($z=0$). The interaction was treated using geometrical optics propagation with inverse bremsstrahlung absorption along the path of propagation. In agreement with the experiment, a dense plasma sidelobe and a density minimum on axis are seen to develop. At 11.2 ns after the initiation of the laser pulse the density in the sidelobe reaches $\sim 5\text{--}6 \times 10^{20} \text{ cm}^{-3}$ at $50 \mu\text{m}$ from the target and $50 \mu\text{m}$ from the axis, and in comparison is $\sim 1 \times 10^{20} \text{ cm}^{-3}$ on axis at the same distance from the target. At $100 \mu\text{m}$ from the target the sidelobe density still has a maximum of $3 \times 10^{20} \text{ cm}^{-3}$. The electron temperature in the axial region irradiated by the laser is computed to increase as a function of time, reaching $> 150 \text{ eV}$ near the time of the peak laser intensity. The plasma in the sidelobe is much colder, with an electron temperature of about 25 eV due to effective radiation cool-

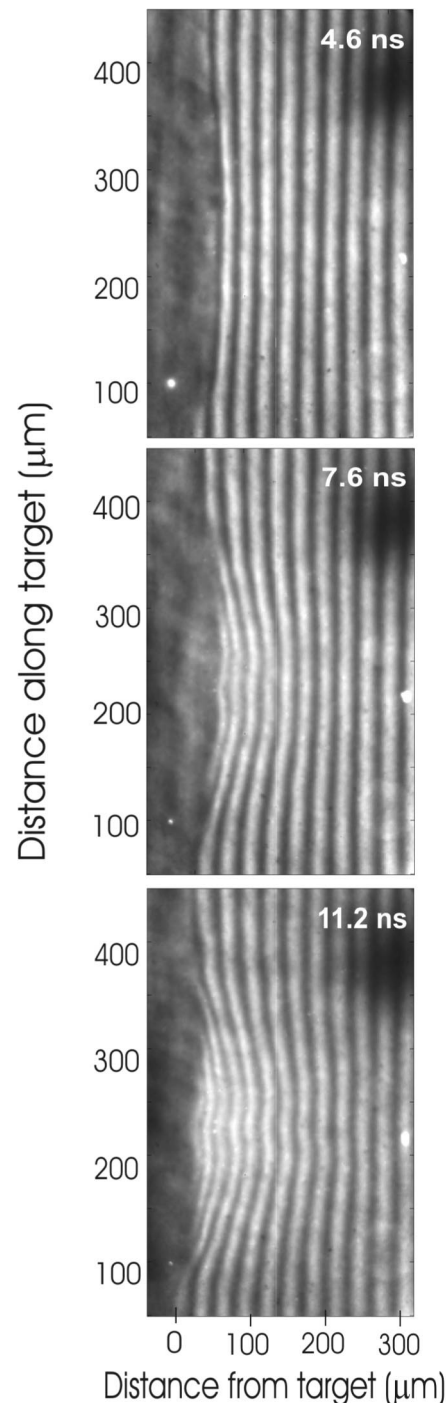


FIG. 6. Sequence of interferograms corresponding to spot-focus plasmas generated by firing a fifth shot in the same target location. The spot diameter was $\sim 30 \mu\text{m}$ and the beam intensity was $7 \times 10^{12} \text{ cm}^{-3}$. The times indicated are measured with respect to the beginning of the laser pulse.

ing. The calculations show that here, as in the case of the previous line focus experiment at lower intensities, radiation pressure effects do not play a significant role in the formation of the observed density profile. The simulations also show that the 1ω laser beam is not strongly refracted, and due to the relatively low laser intensity and small plasma size, laser plasma instabilities are not expected to play a significant role (the stimulated Brillouin scattering growth factor is small),

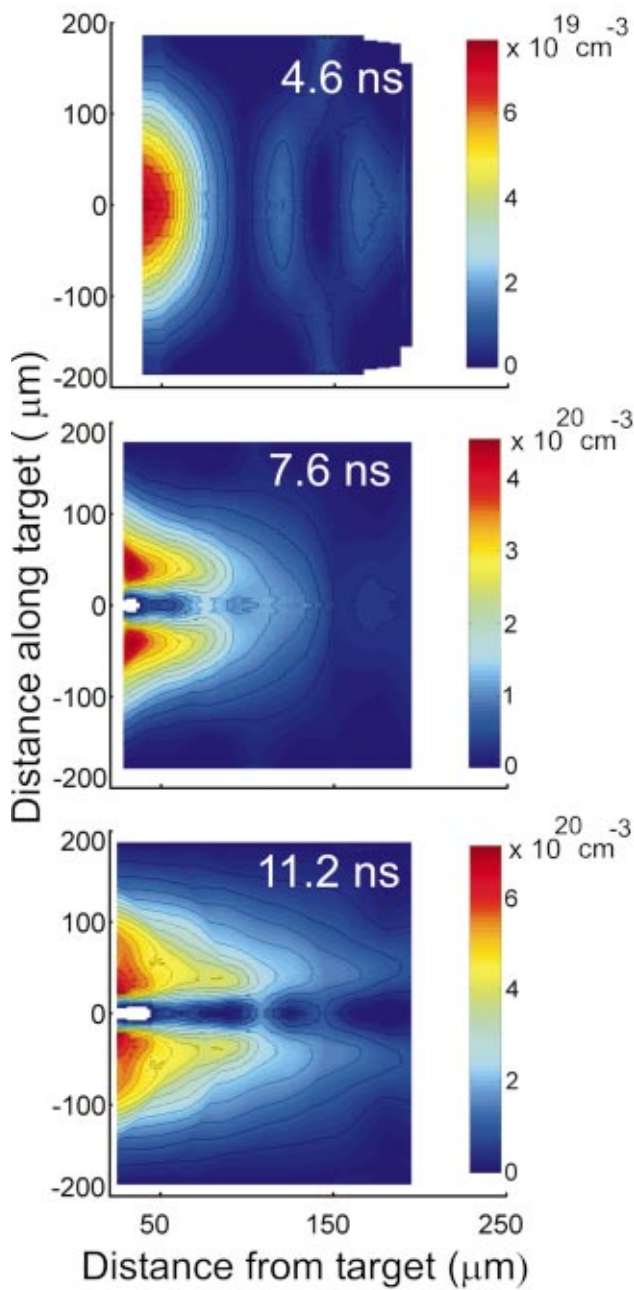


FIG. 7. (Color) Plasma density profiles corresponding to the interferograms of Fig. 6.

and the plasma structure is not caused by filamentation. Instead the “inverted” density profile is a consequence of hydrodynamic and plasma radiation effects.

As is also the case for the line focus experiment, the simulation shows that the density of the sidelobe is significantly increased by plasma radiation-induced ablation of target material from the area surrounding the laser irradiated spot. Plasma radiation is also a major cooling mechanism for the sidelobe plasma. The pressure balance between the two concentric regions contributes to the development of a density depression on axis, similarly to the previously studied case of a line-focus plasma.¹¹ However, the absence of radiation does not stop the “hole formation” in the case of deep

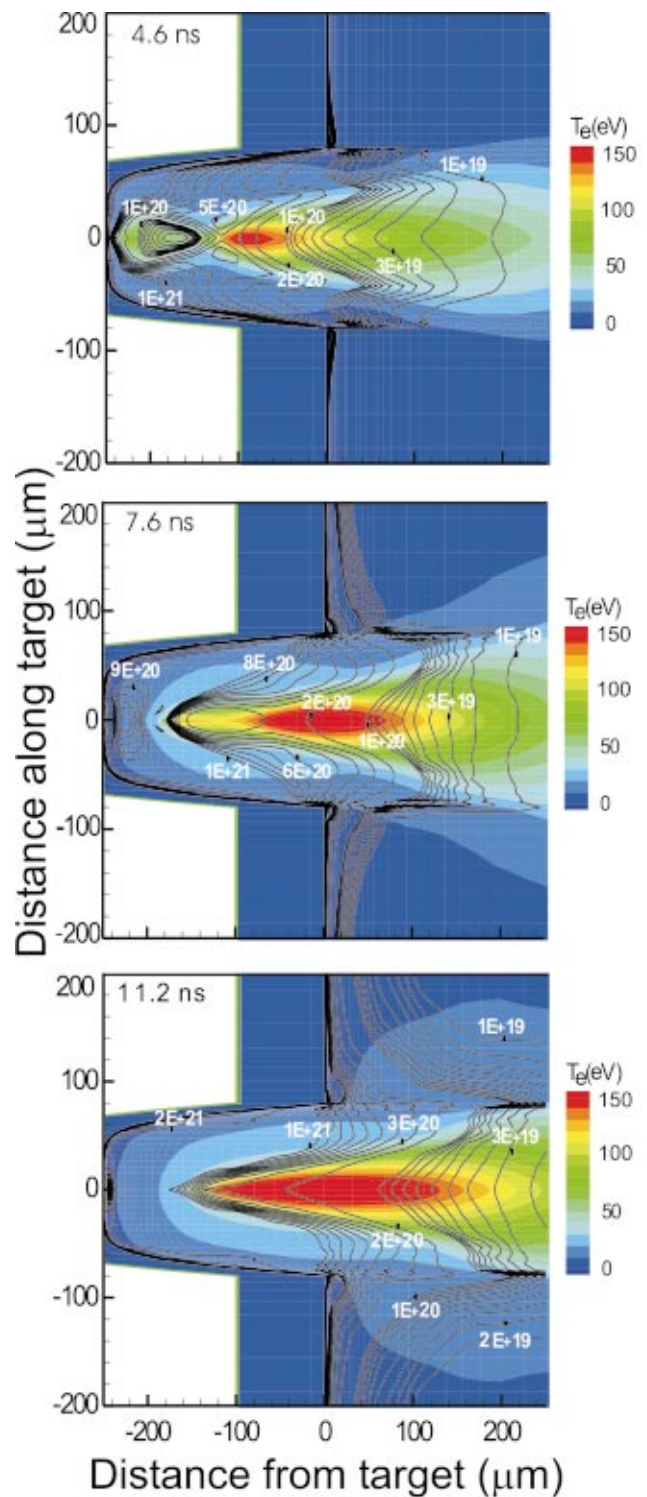


FIG. 8. (Color) Sequence of simulated electron density (line contours) and temperature (filled contour) profiles for the spot-focus plasma of Fig. 7 computed using LASNEX. The 1ω of heating laser is incident from the right.

crater-based plasmas. Across such a relatively narrow crater, pressure balance easily takes place, hence creating a density depression in the hot part along the laser irradiated axis. In other words, the laser pulse is sufficiently long for the interior of the crater to be filled with plasma ablated from the focal spot at the crater’s bottom and for sound waves to transverse the crater dimension multiple times. In addition,

in the present case the crater constrains the plasma expansion in the lateral direction and guides the motion in the direction perpendicular to the target, enhancing the density at large distances from the surface. Plasma radiation adds additional ablated mass, significantly enhancing the magnitude of the plasma density and the depression outside the cavity. The role of plasma radiation was studied by conducting simulations in which either the radiation-induced ablation outside the 30 μm diameter central region or the radiation transport were turned off. It is observed that in the absence of plasma radiation-induced ablation the electron density in the side-lobe is diminished by nearly an order of magnitude at 50 μm from the target (from $\sim 5-6 \times 10^{20} \text{ cm}^{-3}$ at 50 μm from the axis to about $5 \times 10^{19} \text{ cm}^{-3}$ in the same location for the case without plasma radiation-induced ablation). In the case without radiation transport the plasma temperature in the sidelobe is significantly higher, and both the density in the sidelobe and the magnitude of the density depression are significantly reduced.

IV. CONCLUSIONS

Extremely compact soft x-ray lasers with excellent spatial coherence and very high spectral brightness have been developed based on fast capillary discharges. The use of a table-top 46.9 nm laser in plasma interferometry has been demonstrated in several experiments. The potential of these compact short wavelength sources in the diagnostics of dense plasmas is exemplified by interferometry results that unveiled complex two-dimensional effects in the evolution of laser-created plasmas. With a small size, high brightness, narrow linewidth, and excellent spatial coherence table-top soft x-ray lasers are positioned to become an important high resolution tool for the study of high density plasmas and for the validation of hydrodynamic codes.

ACKNOWLEDGMENTS

This work was supported by the U.S. Department of Energy Grant No. DE-FG03-02NA00062 and by the National Science Foundation. Part of this work was performed under the auspices of the U.S. Department of Energy by the University of California, Lawrence Livermore National Laboratory through the Institute of Laser Science and Application, under Contract No. W-7405-Eng-48. We also gratefully acknowledge the support of the W. M. Keck Foundation.

¹I. H. Hutchinson, *Principles of Plasma Diagnostics* (Cambridge University Press, Cambridge, 1987); T. P. Hughes, *Plasmas and Laser Light* (Wiley, New York, 1975).

²L. B. Da Silva, T. W. Barbee, Jr., R. Cauble *et al.*, Phys. Rev. Lett. **74**, 3991 (1995).

³R. Cauble, L. B. Da Silva, J. T. Barbee, P. Celliers, J. C. Moreno, and A. S. Wan, Phys. Rev. Lett. **74**, 3816 (1995).

⁴D. Ress, L. B. Da Silva, R. A. London, J. E. Trebes, S. Mrowka, R. J. Procassini, J. T. W. Barbee, and D. E. Lehr, Science **265**, 514 (1994).

⁵A. S. Wan, T. W. Barbee, R. Cauble, P. Celliers, L. B. DaSilva, J. C. Moreno, P. W. Rambo, G. F. Stone, J. E. Trebes, and F. Weber, Phys. Rev. E **55**, 6293 (1997).

⁶J. J. Rocca, Rev. Sci. Instrum. **70**, 3799 (1999).

⁷M. C. Marconi, C. H. Moreno, J. J. Rocca, V. N. Shlyaptsev, and A. L. Osterheld, Phys. Rev. E **62**, 7209 (2000).

⁸J. J. Rocca, C. H. Moreno, M. C. Marconi, and K. Kanizay, Opt. Lett. **24**, 420 (1999).

⁹C. H. Moreno, M. C. Marconi, K. Kanizay, J. J. Rocca, Yu. A. Uspenskii, A. V. Vinogradov, and Yu. A. Pershin, Phys. Rev. E **60**, 911 (1999).

¹⁰J. Filevich, K. Kanizay, M. C. Marconi, J. L. A. Chilla, and J. J. Rocca, Opt. Lett. **25**, 356 (2000).

¹¹J. Filevich, J. J. Rocca, E. Jankowska, E. C. Hammarsten, M. C. Marconi, S. Moon, and V. N. Shlyaptsev, "Two dimensional effects in laser created plasmas measured with soft x-ray laser interferometry," Phys. Rev. E (to be published).

¹²E. Jankowska, E. C. Hammarsten, B. Szapiro, J. Filevich, M. C. Marconi, and J. J. Rocca, *X-Ray Lasers 2002, 8th International Conference on X-Ray Lasers*, Proc. 641, edited by J. J. Rocca, J. Dunn, and S. Suckewer (American Institute of Physics, Melville, NY, 2002), p. 498.

¹³R. Smith, J. Dunn, J. Nilsen, V. N. Shlyaptsev, S. Moon, J. Filevich, J. J. Rocca, M. C. Marconi, J. R. Hunter, and T. W. Barbee, Jr., Phys. Rev. Lett. **89**, 065004 (2002).

¹⁴B. R. Benware, C. D. Macchietto, C. H. Moreno, and J. J. Rocca, Phys. Rev. Lett. **81**, 5804 (1998).

¹⁵C. D. Macchietto, B. R. Benware, and J. J. Rocca, Opt. Lett. **24**, 1115 (1999).

¹⁶J. Dunn, Y. Li, A. L. Osterheld, J. Nilsen, J. R. Hunter, and V. N. Shlyaptsev, Phys. Rev. Lett. **84**, 4834 (2000).

¹⁷S. Sebban, R. Haroutunian, Ph. Balcou *et al.*, Phys. Rev. Lett. **86**, 3004 (2001).

¹⁸D. V. Korobkin, C. H. Nam, C. H. Suckewer, and A. Goltsov, Phys. Rev. Lett. **77**, 5206 (1996).

¹⁹M. Frati, M. Seminario, and J. J. Rocca, Opt. Lett. **25**, 1022 (2000).

²⁰F. G. Tomasel, J. J. Rocca, V. N. Shlyaptsev, and C. D. Macchietto, Phys. Rev. A **54**, 2474 (1997).

²¹J. J. Rocca, V. N. Shlyaptsev, F. G. Tomasel, O. D. Cortazar, D. Hartshorn, and J. L. A. Chilla, Phys. Rev. Lett. **73**, 2192 (1994).

²²A. V. Vinogradov and V. N. Shlyaptsev, Kvant. Elektron. (Moscow) **10**, 509 (1983) [Sov. J. Quantum Electron **13**, 298 (1983)]; **10**, 2325 (1983) [**13**, 1511 (1983)]; V. N. Shlyaptsev, A. V. Gerusov, A. V. Vinogradov, J. J. Rocca, O. D. Cortazar, F. G. Tomasel, and B. Szapiro, Proc. SPIE **2012**, 99 (1993).

²³J. J. Rocca, D. P. Clark, J. L. A. Chilla, and V. N. Shlyaptsev, Phys. Rev. Lett. **77**, 1476 (1996).

²⁴N. A. Bobrova, S. V. Bulanov, T. L. Razinkova, and P. V. Sasorov, Plasma Phys. Rep. **22**, 349 (1996).

²⁵Y. Liu, M. Seminario, F. G. Tomasel, C. Chang, J. J. Rocca, and D. T. Attwood, Phys. Rev. A **63**, 033802 (2001).

²⁶L. B. Da Silva, T. W. Barbee, Jr., R. Cauble, P. Celliers, D. Ciarlo, J. C. Moreno, S. Mrowka, J. E. Trebes, A. S. Wan, and F. Weber, Appl. Opt. **34**, 6389 (1995).

²⁷F. Albert *et al.*, Opt. Commun. **142**, 184 (1997).

²⁸R. F. Smith, S. Hubert, M. Fajardo *et al.*, in Ref. 12, p. 617.

²⁹Hyperfine Inc., 4946 North 63rd St., Boulder, CO 80301.

³⁰Yu. A. Uspenskii, V. E. Lebashov, A. V. Vinogradov, A. I. Fedorenko, V. V. Kondratenko, Yu. P. Pershing, E. N. Zubalev, and V. Yu Fedotov, Opt. Lett. **23**, 771 (1998).

³¹D. T. Attwood, D. W. Sweeney, J. M. Auerbach, and P. H. Y. Lee, Phys. Rev. Lett. **40**, 184 (1978).

³²S. Wilks, P. E. Young, J. Hammer, M. Tabak, and W. L. Kruer, Phys. Rev. Lett. **73**, 2994 (1994).

³³K. Takahashi, R. Kodama, K. A. Tanaka, H. Hashimoto, Y. Kato, K. Mima, F. A. Weber, T. W. Barbee, and L. B. Da Silva, Phys. Rev. Lett. **84**, 2405 (2000).

³⁴L. A. Bol'shov, I. N. Burdonskii, A. L. Velikovich *et al.*, Sov. Phys. JETP **65**, 1160 (1987).

³⁵B. Rus, P. Zeitoun, T. Mocek *et al.*, Phys. Rev. A **56**, 4229 (1997).

³⁶V. A. Boiko, S. A. Pikuz, and A. Ya. Faenov, Sov. J. Quantum Electron. **5**, 658 (1975).

³⁷G. D. Zimmerman and W. L. Kruer, Comments Plasma Phys. Controlled Fusion **2**, 51 (1975).